Optimal Overlapping Tomography

Kiara Hansenne,[1,2,*] Rui Qu,[3,4,†] Lisa T. Weinbrenner,[1] Carlos de Gois,[1] Haifei Wang,[3,4] Yang Ming,[3] Zhengning Yang,[3] Paweł Horodecki,[5,6] Weibo Gao,[3,4,‡] and Otfried Gühne[1,§]

[1]*Naturwissenschaftlich-Technische Fakultät, Universität Siegen, Walter-Flex-Straße 3, 57068 Siegen, Germany*
[2]*Institut de Physique Théorique, Université Paris-Saclay, CEA, CNRS, 91191 Gif-sur-Yvette, France*
[3]*Division of Physics and Applied Physics, School of Physical and Mathematical Sciences, Nanyang Technological University, Singapore 637371, Singapore*
[4]*Centre for Quantum Technologies, National University of Singapore, Singapore 117543, Singapore*
[5]*Faculty of Applied Physics and Mathematics, Gdańsk University of Technology, 80-233 Gdańsk, Poland*
[6]*International Centre for Theory of Quantum Technologies, University of Gdańsk, Jana Bażyńskiego 1A, 80-309 Gdańsk, Poland*

(Received 23 December 2024; revised 27 June 2025; accepted 14 July 2025; published 4 August 2025)

Characterizing large-scale quantum systems is central to fundamental physics and essential for applications of quantum technologies. While a full characterization requires exponentially increasing resources, focusing on application-relevant information can often lead to significantly simplified analysis. Overlapping tomography is such a scheme, allowing one to obtain all the information contained in specific subsystems of multiparticle quantum systems in an efficient manner, but the ultimate limits of this approach remain elusive. We present protocols for overlapping tomography that are optimal with respect to the number of measurement settings. First, by providing algorithmic approaches based on graph theory we find the minimal number of Pauli settings, relating overlapping tomography to the problem of covering arrays in combinatorics. This significantly reduces the number of measurement settings, showing for instance that two-body overlapping tomography of nearest neighbors in qubit systems with planar topologies can always be performed with nine Pauli settings. Second, we prove that using general projective measurements, all k-body marginals can be reconstructed with only 3^k settings, independently of the system size. Finally, we demonstrate the practical applicability of our methods in a six-photon experiment. Our results will find applications in learning noise and interaction patterns in quantum computers as well as characterizing fermionic systems in quantum chemistry.

DOI: 10.1103/t6qb-kdcp

Extracting relevant information from large-scale quantum systems is key to advancing quantum technologies. Depending on the scenario, this may involve certifying quantum computers [1–4], identifying quantum phase diagrams [5,6], or certifying the topology and robustness of quantum networks [7,8]. Currently, efforts are devoted to Hamiltonian learning [9–14], quantum noise characterization [15–20], or quantum state analysis [21,22], all of which share a feature of locality. Physical Hamiltonians and quantum noise models are often local, involving only few-particle interactions, while quantum states are often well characterized by their few-body marginals. This holds for instance for ground states of gapped few-body Hamiltonians [23–25], states from shallow circuits [26], injective projected entangled pair states [27–29], and in some cases, generic pure states [30,31]. Developing methods to extract such local information is vital, particularly given recent experiments where switching measurement settings requires additional effort [32].

The concept of overlapping tomography addresses this problem. In its original formulation [33–35], the authors aimed to reconstruct every k-body marginal of an n-qubit state ϱ using only Pauli settings, $\{X, Y, Z\}^{\otimes n}$, and showed that this requires a measurement budget increasing only logarithmically in n. This was later extended to nearest-neighbor marginals [36], shown to achieve quadratic improvement when considering repetitions of Pauli settings [37], applied to quantum noise characterization [38,39], and demonstrated experimentally [40].

We generalize overlapping tomography in several aspects and present optimal schemes for it. First, under the Pauli measurement restriction, we propose a graph-theoretic

*Contact author: kiara.hansenne@ipht.fr
†Contact author: rui.qu@ntu.edu.sg
‡Contact author: wbgao@ntu.edu.sg
§Contact author: otfried.guehne@uni-siegen.de

Published by the American Physical Society under the terms of the Creative Commons Attribution 4.0 International license. Further distribution of this work must maintain attribution to the author(s) and the published article's title, journal citation, and DOI.

technique to construct minimal measurement schemes that recover all k-body marginals. This significantly improves upon current solutions and, importantly, extends to cases where only specific marginals are requested. For example, when marginals of nearest neighbors in planar lattices are needed, we show that nine Pauli settings are sufficient, irrespective of the system size. Second, relaxing the Pauli measurement restriction, we consider local qubit rotations and computational basis measurements, which is routine for all major experimental platforms. With projective measurements, a minimum of 3^k settings is required for the state tomography of k-qubit systems. Here, we show that k-body overlapping tomography of n-qubit systems can be performed with that minimum of 3^k settings, independent of system size n. To demonstrate feasibility and scalability, we fully characterize all two-body marginals of a six-photon entangled Dicke state using 12 optimal Pauli settings and nine optimal non-Pauli settings. This nearly halves the requirements of a recent demonstration [40] while generalizing to non-Pauli measurements.

Optimality in the Pauli scheme—For Pauli measurements, overlapping tomography reduces to identifying a set of n-body Pauli settings that allows for the reconstruction of all k-qubit marginal states. While a naive count suggests $3^k\binom{n}{k}$ measurement settings, this approach is highly redundant, as many settings are effectively identical across k-qubit subsets. Overlapping tomography exploits these overlaps to construct much smaller measurement sets. To give a simple example, the nine Pauli settings $XXXX$, $ZYYX$, $YZZX$, $YYXY$, $XZYY$, $ZXZY$, $ZZXZ$, $YXYZ$, and $XYZZ$ (omitting tensor product symbols) suffice to reconstruct all two-qubit marginals, as for every pair of qubits, the nine combinations of Pauli operators occur. The cardinality of such minimal Pauli sets is denoted by $\phi_k(n)$. In the example, the set is optimal, so $\phi_2(4) = 9$.

Our main observation is that this problem can be mapped to a graph-theoretic formulation solvable via binary programming. For simplicity, we focus on reconstructing all two-body marginals of an n-qubit state, with generalizations to subsets of k-body marginals detailed in Appendix A of Supplemental Material (SM) [41].

First, we construct a graph where the edges represent the two-qubit Pauli operators required for reconstructing the marginals. Each qubit is represented by three vertices (one for each Pauli operator), and vertices corresponding to different qubits are fully connected, forming the complete n-partite graph with three nodes per party, $K_{n,3}$ (see Fig. 1 for a three-qubit example). Here, n-body Pauli settings correspond to fully connected vertex sets (cliques) in $K_{n,3}$. Thus, finding minimal Pauli settings is equivalent to finding the smallest set of cliques covering all graph edges.

This can be expressed as a binary optimization program. First, let C and E denote the sets of cliques and edges of the graph $K_{n,3}$, respectively. We then associate each clique $c \in C$ to a variable $z_c \in \{0, 1\}$. Whenever a clique is active

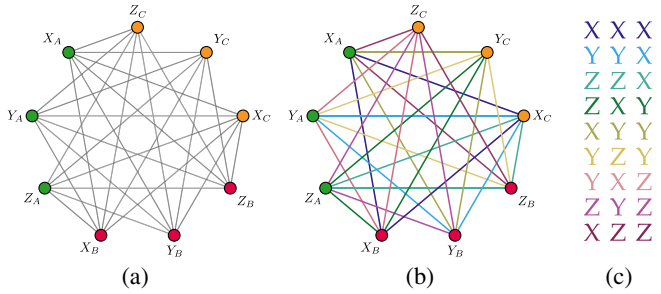


FIG. 1. (a) Measurement graph $K_{3,3}$ for three qubits. Each qubit is represented by three vertices corresponding to the Pauli operators X, Y, and Z. Edges represent two-body Pauli operators, and cliques (triangles) correspond to three-qubit Pauli settings. (b) A minimal edge clique covering of $K_{3,3}$. Each color group edges into a triangle, minimizing the total number of triangles needed to cover all edges. (c) Three-qubit Pauli settings derived from the clique covering, ensuring all two-body Pauli operators for each qubit pair are included. Colors match the triangles in (b).

($z_c = 1$), then the measurement associated to c is part of the solution. Each clique contains several edges, and if clique c is active, all its edges are covered. For a solution to be valid, all the edges of $K_{n,3}$ must be covered. To guarantee this, we associate each edge $e \in E$ to a vector $(e_1, \ldots, e_{|C|})$, where $e_c = 1$ if the edge e is in the clique c; otherwise $e_c = 0$. Then, the condition can be expressed by requiring that $\sum_{c \in C} z_c e_c \geq 1$ for any $e \in E$, meaning that for each edge of the graph, at least one clique that contains it must be in the solution. Altogether, we obtain

$$\phi_2(n) = \min_{\{z_c\}_{c \in C}} \sum_{c \in C} z_c \tag{1a}$$

$$\text{subject to } z_c \in \{0, 1\}, \quad \forall \ c \in C, \tag{1b}$$

$$\sum_{c \in C} z_c e_c \geq 1, \quad \forall \ e \in E. \tag{1c}$$

Equation (1) can be modeled using modeling languages such as JuMP [50] and solved by standard integer programming solvers (see, e.g., Gurobi [51]). The minimal Pauli settings are obtained from the resulting values of z_c. The solutions improve significantly over previous constructions. For example, the four-qubit solution from above improves the best previous Pauli set, which contains 12 Pauli settings to perform two-body overlapping tomography [35]. For six qubits, we obtain $\phi_2(6) = 12$, whereas in Refs. [33,34] and in Ref. [35], 21 and 15 settings are needed respectively (see Appendix A5 of SM [41] for explicit minimal Pauli sets).

We add that this graphical formulation is a specific instance of the edge clique covering problem, which has long been studied in graph theory. For instance, de Caen *et al.* showed in 1985 that $\phi_2(n) \leq 6\lceil \log_3(n) \rceil + 3$ [52], which exactly matches the size of the construction

presented in Ref. [35]. The general formulation of the edge clique covering problem, however, is known to be NP-complete [53]. The similar problem of vertex clique covering has also been explored in the context of Pauli measurement scheduling; see, for instance, Refs. [37,54].

The combinatorial problem underlying overlapping tomography with Pauli measurements corresponds to covering arrays in combinatorial design theory [55,56]. Several facts about the minimal Pauli sets can thus be immediately borrowed, such as bounds on $\phi_k(n)$ and explicit constructions. As examples, it is known that $\phi_k(k+1) = 3^k$, and that $\phi_k(n) \leq (k-1)\{\log[3^k/(3^k - 1)]\}^{-1} \log(n)[1 + o(1)]$ [55,56]. However, minimal covering arrays are notoriously hard to construct: when $k = 2$, covering arrays with three symbols (here, X, Y, and Z, the three Pauli operators) are only known up to $n = 20$ parties [57]. The resulting $\phi_2(n)$ are presented in Fig. 2, and compared to previous constructions [33–35]. The connection to covering arrays for the special case $k = 2$ has been observed before [58–61], and a hypergraph generalization to $k > 2$ is presented in Appendix A2 of SM [41]. Note that Ref. [18] pointed to a connection between covering arrays and graph coloring to the learning of noise models, which turns out to be equivalent to the problem of partial tomography for all k-body marginals.

The advantage of our graphical formulation is twofold. First, the binary program presented in Eq. (1) can directly be extended to higher values of k and can be used to compute, for instance, $\phi_3(4) = 27$ and $\phi_3(5) = \phi_3(6) = 33$ (see Appendix A5 of SM [41]). To the best of our knowledge, it had not been previously shown that covering arrays corresponding to $\phi_3(5) = 33$ were optimal. Second, the graphical formulation is highly flexible: with appropriate modifications, it can be used to obtain minimal Pauli sets to reconstruct not all marginals, but rather only a subset of them. This problem has been coined "local overlapping tomography" [36]. In the graphical formulation, we define the n-vertex connectivity graph G, where vertices are connected if the marginal of the corresponding qubits is desired. We explore this in detail in Appendix A of SM [41] and, notably, we prove that for systems having a connectivity graph with a chromatic number of at most four (such as for instance all planar graphs), two-body overlapping tomography can always be performed with nine Pauli settings, regardless of the number of qubits.

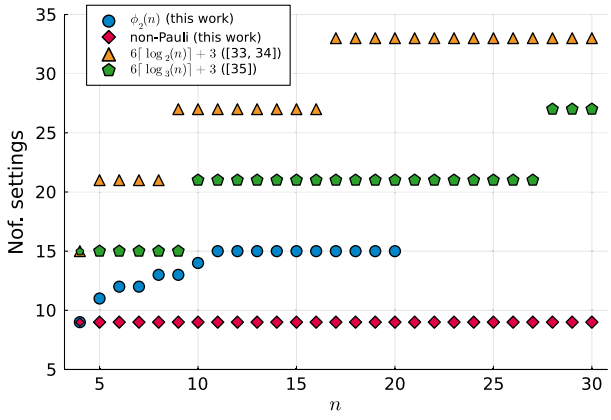


FIG. 2. Number of measurement settings needed for two-body overlapping tomography of n qubits ($k = 2$). Blue circles: minimal number of Pauli settings possible, corresponding to covering array numbers [57]. Red squares: minimal number of projective settings, $3^2 = 9$. Orange triangles: number of Pauli settings needed in the construction of Refs. [33,34]. Green pentagons: number of Pauli settings needed in the construction of Ref. [35].

Optimality beyond Pauli measurements—If the local settings are restricted to Pauli measurements, the number of measurement settings increases with n. To improve this, more general settings than just Pauli measurements can be allowed locally. Indeed, this approach ensures that the minimal number of n-qubit measurement settings, 3^k, can always be reached.

Reconstructing every two-body marginal state can be done by obtaining the expectation values of the nine Pauli observables $\{X, Y, Z\}^{\otimes 2}$ for all pairs of qubits $\{i, j\}$. In terms of Bloch vectors, this means that the two parties choose their measurement directions on the Bloch sphere to be exactly the standard basis $\{\vec{e}_m\}_{m=1}^3$ in three-dimensional real space, and measure all possible combinations

$$\mathcal{M}_{m,l} = \vec{e}_m \otimes \vec{e}_l, \tag{2}$$

where the observables can be obtained from this shorthand notation by setting $\vec{v} \mapsto v_1 X + v_2 Y + v_3 Z$.

To obtain tomographically complete information on the two-qubit marginal, it is not important that the nine vectors $\vec{e}_m \otimes \vec{e}_l$ are orthogonal. They simply need to be linearly independent and thus form a basis. So, the key idea is to randomly choose nine observables for each party instead of the fixed Pauli settings. We denote the respective local measurement directions on the Bloch sphere by $\vec{v}_\alpha^{(i)}$ for all $\alpha \in \{1, \ldots, 9\}$, where i labels the party. Intuitively, if those vectors are chosen independently and according to the uniform distribution on the unit sphere, the nine product vectors $\vec{v}_\alpha^{(i)} \otimes \vec{v}_\alpha^{(j)}$ for the pair $\{i, j\}$ should be linearly independent with unit probability. Since each party chooses their measurement directions randomly, the above argument holds for every possible pair of qubits.

This reasoning suggests that choosing nine random measurement directions $\vec{v}_\alpha^{(i)}$ for each of the n qubits and measuring

$$\mathcal{M}_\alpha = \bigotimes_{i=1}^{n} \vec{v}_\alpha^{(i)}, \qquad \alpha = 1, \ldots, 9 \tag{3}$$

is sufficient to reconstruct all the two-body marginal states of the n-qubit system. In Appendix B of SM [41] we show that this intuition indeed holds true for arbitrary k. Remarkably, the proof holds for arbitrary local dimension d, which shows that k-body overlapping tomography of qudit systems can be performed with $(d^2-1)^k$ settings. Notice also that the resulting measurements are projective and local and therefore do not impose extra experimental requirements. For completeness, this minimal number of settings is also plotted in Fig. 2.

Although random measurement directions yield tomographically complete settings for all marginals, some settings perform better than others regarding statistical errors. Measurement directions that are too close to each other can lead to large variances in the reconstructed states, particularly when the state is nearly orthogonal to all the measurement directions. To assess the quality of a particular set of measurement directions, we use confidence regions informed by measurements variances. Specifically, we use the confidence region C_A from Ref. [62] as a figure of merit, which is straightforward to construct for any measurement scheme. Numerically optimized measurement directions and performance comparisons are provided in Appendixes C and D of SM [41].

Experimental demonstration—We experimentally perform two-body overlapping tomography on a six-photon Dicke state with three excitations, that is,

$$|D_6^{(3)}\rangle = \frac{1}{\sqrt{20}}\sum_i \mathcal{P}_i(|HHHVVV\rangle), \tag{4}$$

where $|H\rangle$ ($|V\rangle$) denotes the horizontal (vertical) polarization and $\sum_i \mathcal{P}_i(\ldots)$ denotes the sum over all 20 permutations leading to different terms. Dicke states are highly entangled multipartite states, widely recognized for their applications in quantum metrology [63,64] and quantum networks [65–67]. Moreover, all their marginal states are entangled [68], which motivates using a Dicke state to demonstrate the practicality of overlapping tomography.

The setup of the experiment, described in detail in Fig. 3, is registering $|D_6^{(3)}\rangle$ with a sixfold coincidence count rate of 7.0 counts per minute. To verify the proper working of our source, we measure the structures in the X, Y, and Z bases and observe the characteristic features of the Dicke state $|D_6^{(3)}\rangle$ [69,70], which is detailed in Appendix E1 of SM [41].

To conduct the six-qubit full state tomography, 729 Pauli settings would need to be measured, making the measurement time prohibitively long. Carrying out optimal two-body overlapping tomography in the Pauli scheme requires $\phi_2(6) = 12$ settings only (see Appendix A5 of SM [41] for the specific measurements). We perform these 12 Pauli measurement settings with an acquisition time for each measurement setting of 2 h. By using maximum likelihood

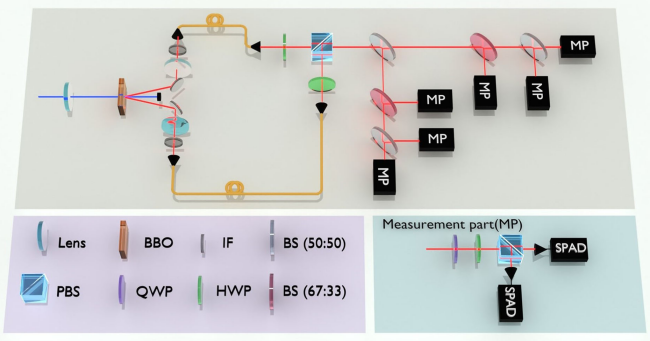


FIG. 3. Experimental setup for generating and detecting six-photon Dicke state with three excitations. Ultraviolet pulses (390 nm, 80 MHz repetition rate, 300 mW average power) are focused onto a type-II beamlike β-barium borate (BBO) crystal using a lens ($f_1 = 75$ mm) to generate three photon pairs photons simultaneously in the third-order spontaneous parametric down-conversion emissions. The photons are recollimated with two lenses ($f_2 = 100$ mm), spectrally and spatially filtered by interference filters (IFs) ($\Delta\lambda = 10$ nm) and single-mode fibers, and merged into a single path by a polarizing beam splitter (PBS). Hong-Ou-Mandel-type interference visibility is 0.92. The six indistinguishable photons are distributed into six output modes using three 50:50 and two 67:33 beam splitters (BSs), achieving a maximal success probability of $5/324$ for detecting one photon in each measurement part (MP). Arbitrary polarization analysis in each output mode is conducted by the MP, composed of a quarter-wave plate (QWP), a half-wave plate (HWP), a PBS, and two single-photon avalanche detectors (SPADs).

estimation [71,72], we reconstruct the physical experimental density matrices of all 15 two-qubit subsystems $\varrho^{\mathrm{P}}_{i_1,i_2}$, where $i_1, i_2 \in \{0,1,\ldots,5\}$. Figure 4(a) depicts the reconstructed marginals of $\varrho^{\mathrm{P}}_{2,3}$ for the Pauli scheme.

Second, we perform the measurements with the nine non-Pauli directions described in the previous section. The acquisition time for each measurement setting is also set to 2 h. Similarly, we reconstructed all two-body marginals $\varrho^{\mathrm{N}}_{i_1,i_2}$ in the non-Pauli scheme, e.g., $\varrho^{\mathrm{N}}_{2,3}$ presented in Fig. 4(b). The method of reconstruction and all experimental marginals for both schemes are presented in Appendix E2 of SM [41].

Subsequently, in order to obtain error estimates, we perform 100 Poisson distribution samples on the experimental sixfold data using a Monte Carlo approach. We obtain the experimental mixed state fidelities $F_{i_1,i_2} = [\mathrm{Tr}(\sqrt{\sqrt{\varrho_{i_1,i_2}}\varrho^{\mathrm{exp}}_{i_1,i_2}\sqrt{\varrho_{i_1,i_2}}})]^2$ and their error bars, where $\varrho_{i_1,i_2} = \mathrm{Tr}_{j_1,j_2,j_3,j_4}(|D_6^{(3)}\rangle\langle D_6^{(3)}|)$ denotes the ideal two-body marginals and $\{j_1,j_2,j_3,j_4\} = \{0,1,\ldots,5\}\backslash\{i_1,i_2\}$. As shown in Fig. 4(a), for the Pauli scheme, the average experimental fidelity of the 15 two-body marginals is 0.909 and the minimum fidelity is 0.887. The average error bar is 0.013. By contrast, Ref. [40] performed 21 Pauli settings on a six-qubit GHZ state for around 80 h to reconstruct its

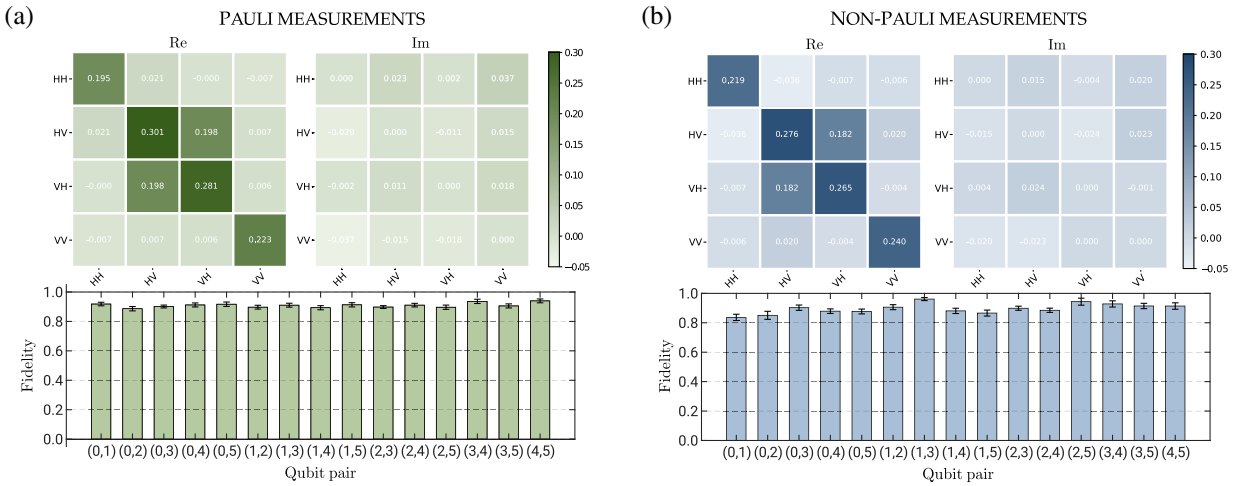


FIG. 4. Two-qubit reduced states from overlapping tomography of a six-qubit Dicke state. (a) Results for the optimal Pauli scheme (12 settings): the real and imaginary parts of the marginal $\varrho^P_{2,3}$ are shown (see Appendix E of SM [41] for other marginals), along with the two-qubit mixed state fidelities between experimental states $\varrho^P_{i_1,i_2}$ and ideal marginals ϱ_{i_1,i_2} for each pair. (b) Similar analysis for the minimal non-Pauli scheme (nine settings). In both cases, fidelity error bars indicate $\pm 1\sigma$ uncertainties estimated via Monte Carlo sampling with Poissonian photon statistics.

two-body marginals, achieving an average fidelity of 0.848 ± 0.013.

Figure 4(b) shows that the average fidelity of reconstructed two-body marginals for non-Pauli Scheme is 0.896 and the average error bar is 0.018. We also observe that requiring a minimal number of nine non-Pauli settings comes at the cost of slightly larger error bars with the same acquisition time for each setting, which is further discussed in Appendix E3 of SM [41]. Our findings demonstrate in theory and in practice that overlapping tomography can be used to drastically reduce experimental requirements, both in the number of measurement settings and measurement time.

Discussion—In this Letter, we have addressed the problem of optimizing measurement scheduling for marginal tomography, combining theoretical analysis with experimental validation. On a purely mathematical side, the connections to graph theory and combinatorics may be used to tackle problems in quantum information theory from a novel perspective. For example, the concept of covering arrays generalizes orthogonal arrays, which have recently led to substantial progress in the study of absolutely maximally entangled states [73], leading to the solution of one of the five central open problems in quantum information theory [74,75]. These connections demonstrate the potential of interdisciplinary approaches in quantum information theory.

On a more practical side, the presented optimal protocols are expected to find applications in quantum simulations, such as the characterization of local Hamiltonians [9–14]. They can also be used for analyzing noise and imperfections in realistic quantum computing devices [15–20]. In addition, these techniques can be extended to measure few-body correlations in fermionic or bosonic systems, as well as to characterize and certify quantum gates in different registers of a quantum computing architecture in parallel. The general applicability of our approach to systems of any size and geometry highlights partial quantum tomography's potential as a scalable and efficient tool for addressing key challenges in large-scale quantum information processing.

Acknowledgments—We thank Adrian Aasen, Maximilian Hess, Jose Este Jaloveckas, Matthias Kleinmann, Chau Nguyen, Lilly Palackal, Martin Plávala, Jonathan Steinberg, Konrad Szymański, Ewout van den Berg, Pawel Wocjan, and Xiao-Dong Yu for discussions. We acknowledge the use of ChatGPT, which helped us identify the existing terminology "covering arrays" in relation to one of our combinatorial problems. This work has been supported by the Deutsche Forschungsgemeinschaft (DFG, German Research Foundation, Projects No. 447948357 and No. 440958198, the Sino-German Center for Research Promotion (Project M-0294), and the German Ministry of Education and Research (Project QuKuK, BMBF Grant No. 16KIS1618K). R. Q., H. W., Y. M., Z. Y., and W. G. acknowledge Singapore Quantum engineering program (NRF2022-QEP2-02-P14). K. H., L. T. W., and C. de G. acknowledge support by the House of Young Talents of the University of Siegen.

Data availability—The data that support the findings of this Letter are not publicly available. The data are available from the authors upon reasonable request.

[1] A. Broadbent, Theory Comput. **14**, 1 (2018).
[2] A. Gheorghiu, T. Kapourniotis, and E. Kashefi, Theory Comput. Syst. **63**, 715 (2018).

[3] J. Carrasco, M. Langer, A. Neven, and B. Kraus, arXiv:2308.11368.
[4] T. Proctor, K. Young, A. D. Baczewski, and R. Blume-Kohout, arXiv:2407.08828.
[5] B. S. Rem, N. Käming, M. Tarnowski, L. Asteria, N. Fläschner, C. Becker, K. Sengstock, and C. Weitenberg, Nat. Phys. **15**, 917–920 (2019).
[6] K. Kottmann, P. Huembeli, M. Lewenstein, and A. Acín, Phys. Rev. Lett. **125**, 170603 (2020).
[7] L. T. Weinbrenner, N. Prasannan, K. Hansenne, S. Denker, J. Sperling, B. Brecht, C. Silberhorn, and O. Gühne, Phys. Rev. Lett. **132**, 240802 (2024).
[8] Y.-L. Mao, H. Chen, B. Guo, S. Liu, Z.-D. Li, M.-X. Luo, and J. Fan, Phys. Rev. Lett. **132**, 240801 (2024).
[9] J. Wang, S. Paesani, R. Santagati, S. Knauer, A. A. Gentile, N. Wiebe, M. Petruzzella, J. L. O'Brien, J. G. Rarity, A. Laing, and M. G. Thompson, Nat. Phys. **13**, 551 (2017).
[10] T. J. Evans, R. Harper, and S. T. Flammia, arXiv:1912.07636.
[11] V. Gebhart, R. Santagati, A. A. Gentile, E. M. Gauger, D. Craig, N. Ares, L. Banchi, F. Marquardt, L. Pezzè, and C. Bonato, Nat. Rev. Phys. **5**, 141 (2023).
[12] H.-Y. Huang, Y. Tong, D. Fang, and Y. Su, Phys. Rev. Lett. **130**, 200403 (2023).
[13] T. Olsacher, T. Kraft, C. Kokail, B. Kraus, and P. Zoller, Quantum Sci. Technol. **10**, 015065 (2024).
[14] D. Stilck França, L. A. Markovich, V. Dobrovitski, A. H. Werner, and J. Borregaard, Nat. Commun. **15**, 311 (2024).
[15] G. O. Samach, A. Greene, J. Borregaard, M. Christandl, J. Barreto, D. K. Kim, C. M. McNally, A. Melville, B. M. Niedzielski, Y. Sung *et al.*, Phys. Rev. Appl. **18**, 064056 (2022).
[16] E. Van Den Berg, Z. K. Minev, A. Kandala, and K. Temme, Nat. Phys. **19**, 1116 (2023).
[17] J. E. Jaloveckas, M. T. P. Nguyen, L. Palackal, J. M. Lorenz, and H. Ehm, arXiv:2311.11639.
[18] E. van den Berg and P. Wocjan, Quantum **8**, 1556 (2024).
[19] T. Wagner, H. Kampermann, D. Bruß, and M. Kliesch, Phys. Rev. Lett. **130**, 200601 (2023).
[20] A. Raza, M. C. Caro, J. Eisert, and S. Khatri, arXiv:2406.04250.
[21] H.-Y. Huang, R. Kueng, and J. Preskill, Nat. Phys. **16**, 1050 (2020).
[22] H. C. Nguyen, J. L. Bönsel, J. Steinberg, and O. Gühne, Phys. Rev. Lett. **129**, 220502 (2022).
[23] H. L. Haselgrove, M. A. Nielsen, and T. J. Osborne, Phys. Rev. Lett. **91**, 210401 (2003).
[24] F. Huber and O. Gühne, Phys. Rev. Lett. **117**, 010403 (2016).
[25] S. Karuvade, P. D. Johnson, F. Ticozzi, and L. Viola, Phys. Rev. A **99**, 062104 (2019).
[26] N. Yu and T.-C. Wei, arXiv:2303.08938.
[27] D. Perez-Garcia, F. Verstraete, M. Wolf, and J. Cirac, Quantum Inf. Comput. **8**, 650 (2008).
[28] A. Molnar, Y. Ge, N. Schuch, and J. I. Cirac, J. Math. Phys. (N.Y.) **59**, 021902 (2018).
[29] J. I. Cirac, D. Perez-Garcia, N. Schuch, and F. Verstraete, Rev. Mod. Phys. **93**, 045003 (2021).
[30] N. Linden, S. Popescu, and W. K. Wootters, Phys. Rev. Lett. **89**, 207901 (2002).
[31] N. S. Jones and N. Linden, Phys. Rev. A **71**, 012324 (2005).
[32] N. Friis, O. Marty, C. Maier, C. Hempel, M. Holzäpfel, P. Jurcevic, M. B. Plenio, M. Huber, C. Roos, R. Blatt, and B. Lanyon, Phys. Rev. X **8**, 021012 (2018).
[33] J. Cotler and F. Wilczek, Phys. Rev. Lett. **124**, 100401 (2020).
[34] X. Bonet-Monroig, R. Babbush, and T. E. O'Brien, Phys. Rev. X **10**, 031064 (2020).
[35] G. García-Pérez, M. A. C. Rossi, B. Sokolov, E.-M. Borrelli, and S. Maniscalco, Phys. Rev. Res. **2**, 023393 (2020).
[36] B. G. M. Araújo, M. M. Taddei, D. Cavalcanti, and A. Acín, Phys. Rev. A **106**, 062441 (2022).
[37] O. Veltheim and E. Keski-Vakkuri, Phys. Rev. Lett. **134**, 030801 (2025).
[38] F. B. Maciejewski, F. Baccari, Z. Zimborás, and M. Oszmaniec, Quantum **5**, 464 (2021).
[39] J. Tuziemski, F. B. Maciejewski, J. Majsak, O. Słowik, M. Kotowski, K. Kowalczyk-Murynka, P. Podziemski, and M. Oszmaniec, arXiv:2311.10661.
[40] Z. Yang, S. Ru, L. Cao, N. Zheludev, and W. Gao, Phys. Rev. Lett. **130**, 050804 (2023).
[41] See Supplemental Material at http://link.aps.org/supplemental/10.1103/t6qb-kdcp for the appendices, which includes Refs. [42–49].
[42] K. Appel and W. Haken, Sci. Am. **237**, 108 (1977).
[43] A. Bretto, *Hypergraph Theory*, Mathematical Engineering (Springer, Cham, 2013).
[44] N. P. K. and S. R. Kola, AKCE Int. J. Graphs Comb. **16**, 230 (2019).
[45] C. Colbourn, Covering array tables for $t = 2, 3, 4, 5, 6$, https://www.public.asu.edu/ ccolbou/src/tabby/catable.html.
[46] J. Torres-Jimenez, Uniform CA, https://www.tamps.cinvestav.mx/oc/.
[47] H. Markowits, J. Finance **7**, 71 (1952).
[48] A. S. Hedayat, N. J. A. Sloane, and J. Stufken, *Orthogonal Arrays*, Springer Series in Statistics (Springer, New York, NY, 1999).
[49] N. J. A. Sloane, A library of orthogonal arrays, http://neilsloane.com/oadir/.
[50] M. Lubin, O. Dowson, J. Dias Garcia, J. Huchette, B. Legat, and J. P. Vielma, Math. Program. Comput. **15**, 581 (2023).
[51] Gurobi Optimization, LLC, Gurobi Optimizer Reference Manual (2024).
[52] D. de Caen, D. A. Gregory, and N. J. Pullman, in *North-Holland Mathematics Studies* (Elsevier, New York, 1985), Vol. 115, pp. 257–267.
[53] J. Orlin, in *Indagationes Mathematicae (Proceedings)* (1977), Vol. 80, pp. 406–424, 10.1016/1385-7258(77)90055-5.
[54] V. Verteletskyi, T.-C. Yen, and A. F. Izmaylov, J. Chem. Phys. **152**, 124114 (2020).
[55] C. J. Colbourn, Le Matematiche **59**, 125 (2004), https://lematematiche.dmi.unict.it/index.php/lematematiche/article/view/166.
[56] J. Torres-Jimenez and I. Izquierdo-Marquez, in *2013 15th International Symposium on Symbolic and Numeric Algorithms for Scientific Computing, Timisoara, Romania* (IEEE, 2013), pp. 20–27, 10.1109/SYNASC.2013.10.
[57] J. I. Kokkala, K. Meagher, R. Naserasr, K. J. Nurmela, P. R. Östergård, and B. Stevens, J. Comb. Des. **28**, 5 (2020).

[58] M. Hou, P. Berman, L. Zhang, and W. Miller, in *Algorithms in Bioinformatics: 6th International Workshop, WABI 2006, Zurich, Switzerland, 2006. Proceedings 6* (Springer, New York, 2006), pp. 138–149.
[59] E. Maltais, Covering arrays avoiding forbidden edges and edge clique covers, Ph.D. thesis, University of Ottawa (Canada), 2009.
[60] A. H. Ronneseth and C. J. Colbourn, Discrete Appl. Math. **157**, 2177 (2009).
[61] P. Danziger, E. Mendelsohn, L. Moura, and B. Stevens, Theor. Comput. Sci. **410**, 5403 (2009).
[62] C. de Gois and M. Kleinmann, Phys. Rev. A **109**, 062417 (2024).
[63] G. Tóth, Phys. Rev. A **85**, 022322 (2012).
[64] Z. H. Saleem, M. Perlin, A. Shaji, and S. K. Gray, Phys. Rev. A **109**, 052615 (2024).
[65] R. Prevedel, G. Cronenberg, M. S. Tame, M. Paternostro, P. Walther, M. S. Kim, and A. Zeilinger, Phys. Rev. Lett. **103**, 020503 (2009).
[66] A. Chiuri, C. Greganti, M. Paternostro, G. Vallone, and P. Mataloni, Phys. Rev. Lett. **109**, 173604 (2012).
[67] W. Roga, R. Ikuta, T. Horikiri, and M. Takeoka, Phys. Rev. A **108**, 012612 (2023).
[68] S. Szalay and P. Nyári, arXiv:2502.18574.
[69] W. Wieczorek, R. Krischek, N. Kiesel, P. Michelberger, G. Tóth, and H. Weinfurter, Phys. Rev. Lett. **103**, 020504 (2009).
[70] C. Schwemmer, G. Tóth, A. Niggebaum, T. Moroder, D. Gross, O. Gühne, and H. Weinfurter, Phys. Rev. Lett. **113**, 040503 (2014).
[71] D. F. V. James, P. G. Kwiat, W. J. Munro, and A. G. White, Phys. Rev. A **64**, 052312 (2001).
[72] J. B. Altepeter, E. R. Jeffrey, and P. G. Kwiat, Adv. At. Mol. Opt. Phys. **52**, 105 (2005).
[73] D. Goyeneche, Z. Raissi, S. Di Martino, and K. Życzkowski, Phys. Rev. A **97**, 062326 (2018).
[74] P. Horodecki, L. Rudnicki, and K. Życzkowski, PRX Quantum **3**, 010101 (2022).
[75] S. A. Rather, A. Burchardt, W. Bruzda, G. Rajchel-Mieldzioć, A. Lakshminarayan, and K. Życzkowski, Phys. Rev. Lett. **128**, 080507 (2022).